Article

Analysis of Transformation Methods of Hydroacoustic and Optoelectronic Data Based on the Tombolo Measurement Campaign in Sopot [†]

Oktawia Lewicka [1], Mariusz Specht [2,*], Andrzej Stateczny [3], Cezary Specht [1], Czesław Dyrcz [4], Paweł Dąbrowski [1], Bartosz Szostak [3], Armin Halicki [2], Marcin Stateczny [2] and Szymon Widźgowski [2]

[1] Department of Geodesy and Oceanography, Gdynia Maritime University, Morska 81–87, 81–225 Gdynia, Poland; o.lewicka@wn.umg.edu.pl (O.L.); c.specht@wn.umg.edu.pl (C.S.); p.dabrowski@wn.umg.edu.pl (P.D.)

[2] Marine Technology Ltd., Wiktora Roszczynialskiego 4–6, 81–521 Gdynia, Poland; a.halicki@marinetechnology.pl (A.H.); m.stateczny@marinetechnology.pl (M.S.); s.widzgowski@marinetechnology.pl (S.W.)

[3] Department of Geodesy, Gdańsk University of Technology, Gabriela Narutowicza 11–12, 80–233 Gdańsk, Poland; andrzej.stateczny@pg.edu.pl (A.S.); b.szostak@marinetechnology.pl (B.S.)

[4] Department of Navigation and Maritime Hydrography, Polish Naval Academy, Śmidowicza 69, 81–127 Gdynia, Poland; c.dyrcz@amw.gdynia.pl

* Correspondence: m.specht@marinetechnology.pl

[†] This article is an extended version of our abstract published in Proceedings of the 15th Baška GNSS Conference: Technologies, Techniques and Applications Across PNT and the 2nd Workshop on Smart, Blue and Green Maritime Technologies, Baška, Croatia, 8–13 May 2022; pp. 17–20.

Abstract: Measurements in the coastal zone are carried out using various methods, including Global Navigation Satellite Systems (GNSS), hydroacoustic and optoelectronic methods. Therefore, it is necessary to develop coordinate transformation models that will enable the conversion of data from the land and marine parts to one coordinate system. The article presents selected issues related to the integration of geodetic and hydrographic data. The aim of this publication is to present the various transformation methods and their effects that relate to the data from the tombolo measurement campaign in Sopot conducted in 2018. Data obtained using GNSS Real Time Kinematic (RTK) measurements, Terrestrial Laser Scanning (TLS), the Unmanned Aerial Vehicle (UAV) and the Unmanned Surface Vehicle (USV) were transformed. On the basis of the coordinate transformation methods used, it can be concluded that the adjustment calculus method obtained the best results for the plane coordinates, while the method of P.S. Dąbrowski et al. obtained the best results for the height coordinates. The standard deviation for the difference of the modelled coordinates acquired by the method of P.S. Dąbrowski et al. with respect to the reference coordinates amounted to: 0.022 m (Northing), 0.040 m (Easting) and 0.019 m (height), respectively, while the adjustment calculus method allowed to obtain the following values: 0.009 m (Northing), 0.005 m (Easting) and 0.359 m (height). It can be assumed that a combination of these two seven-parameter transformation methods would provide the best results. In the future, a new seven-parameter transformation method should be developed based on the synthesis of these two existing methods.

Keywords: data integration; hydroacoustic methods; optoelectronic methods; tombolo; Unmanned Aerial Vehicle (UAV); Unmanned Surface Vehicle (USV)

1. Introduction and Background

Hydroacoustic and optoelectronic methods are increasingly used in shallow water-body surveys [1]. This is due to the continuous development of measuring devices and systems that provide high-quality hydrographic data [2]. Hydroacoustic devices, mainly

echo sounders, are used in most the hydrographic surveys [3,4]. The operation of hydro-acoustic devices [5] is based on the phenomenon of acoustic location. The system sends out a high-frequency sound wave into the water and then records the vibrations of the wave reflected off the bottom. The time and velocity of the sent sound wave enable the calculation of the depth at a selected bottom point. However, in the coastal zone measurements, optoelectronic devices are also used [6]. This is due to the fact that hydroacoustic devices are unable to measure the area of the water adjacent to the coastline. The operation of optoelectronic devices involves the conversion of electrical signals into optical signals and of optical signals into electrical signals. One of the optoelectronic devices that provides very dense and accurate spatial data of the coastal zone is the Airborne LiDAR Bathymetry (ALB) [7]. Its operation is based on the application of green lasers, and the depth value itself is determined through the knowledge of the two-directional course of a laser beam between the water surface and the reflections from the seabed located underneath [8,9]. In research, a Terrestrial Laser Scanner (TLS) is also used. This is a ground-based, active imaging method that rapidly acquires accurate, dense 3D point clouds of object surfaces by laser range-finding. Another optoelectronic technique that enables the received bathymetric data is photogrammetry and remote sensing [10,11]. Due to the dynamic development of Unmanned Aerial Vehicle (UAV) technology, various unmanned platforms equipped with cameras are used often in the measurement. In these techniques, a photo provides information about the depth of the waterbody.

However, with advances in technology, the problem of geospatial data integrity has emerged. Ref. [12] presents a new method for integrating data acquired by UAVs and Unmanned Surface Vehicles (USVs). This method is based on the processing of two data sets, from UAVs and USVs, using a bathymetric reference surface and the selection of points on the basis of generated masks. Processed data in the LAS format file create a digital surface using different interpolation methods. An important element of the proposed method is the acquisition of UAV data using underwater Ground Control Points (GCP). The data from the UAV platform were processed in the Pix4D Mapper. HYPACK 2021 hydrographic software was responsible for the integration of bathymetric and position data from the USV. A similar method is described in [13]. This study presents the development of a surface model based on data acquired on an UAV carrying an aerial optical sensor for photogrammetry and with an Autonomous Surface Vehicle (ASV) expressly addressed to work in extremely shallow water with underwater acoustic sensors. The bathymetric and topographic data merged together on the basis of the calculated control points and the digitised shoreline between the two data sets. Data merging was performed by using a dedicated tool in the Geographic Information System (GIS) [14] that provides a single continuous model. In this study, the process of georeferencing the UAV was obtained by the Agisoft Metashape software [15]. Another method that was developed on the basis of the UAV and USV measurements was described by [16]. One of the assumptions of the study was to generate a topographic terrain model from the images covering the estuary area using the Structure-from-Motion (SfM) method [17] and the interpolation of the bathymetric point cloud. The UAV cloud had georeferencing from the control points; however, the bathymetric data did not require georeferencing because they were assigned coordinates from the Global Navigation Satellite System (GNSS) receiver. Ref. [18] proposed a new approach to shallow water bathymetry mapping that integrates hyperspectral image and sparse sonar data, allowing for the extraction of homogeneous regions from hyperspectral images and the interpolation of sonar points in each homogeneous region.

Undoubtedly, coordinate transformation is one of the computational tasks frequently encountered during map compilation. Currently, this is done using programs and tools such as ArcGIS, CloudCompare, Eye4Software Coordinate Calculator or VDatum [19], which have facilitated the processing of data. However, they have limitations resulting from the availability of the transformation methods and their modifiability.

It is also worth paying attention to the tombolo oceanographic phenomenon, conducted in Sopot in 2018 [20–22], which carried out bathymetric surveys using a GNSS receiver, TLS, UAV and an USV. The data recorded by TLS had a local coordinate system, while the GNSS receiver and the USV recorded the position coordinates in the national PL–2000 system (EPSG:2177) and the normal heights in the PL–KRON86–NH system. Thanks to the navigation module, the UAV point cloud received georeferencing in the form of coordinates of the Polish national PL–2000 plane coordinate system and ellipsoidal heights.

In view of the above, the transformation of coordinates is an issue that should be discussed systematically, as it will then include the current formats and types of recording coordinates derived from commercially available geodetic and hydrographic devices and systems. Moreover, the coordinate conversion is related to the existing legislation in Poland. Pursuant to Regulation [23], §24(1) of [24] shall be read as follows: "The PL–KRON86–NH height system shall be used until the implementation of the PL–EVRF2007–NH height system entire the country, but no later than 31 December 2023". As of 31 January 2022, the PL–EVRF2007–NH system has been introduced in 253 poviats (districts), while in 108 poviats, implementation work is in progress, which means that the height system valid in Poland is the PL–KRON86–NH system. It is therefore reasonable to provide height data in both the PL–EVRF2007–NH and PL–KRON86–NH systems. Another document in force in Poland, which specifies valid spatial reference systems, is the Regulation [24], according to which the hydrographic work documentation for the purposes of issuing nautical charts shall be prepared in the PL–UTM (Universal Transverse Mercator) plane coordinate system. This means that when preparing bathymetric charts obtained from devices recording in different reference systems, it is required that all the data be transformed to the PL–UTM system and PL–EVRF2007–NH or PL–KRON86–NH system.

Another document that provides for data standardisation is the INSPIRE Directive [25]. The main objective of the Directive is to ensure the public availability of spatial information through the creation of the spatial information infrastructure. It assumes the possibility of combining, in a uniform way, spatial data derived from different sources. Data harmonisation is a way to achieve this aims, which requires that data transformation processes be carried out.

The main objective of this paper is to present selected coordinate transformation methods and their use for the data derived from surveys of the tombolo oceanographic phenomenon, carried out in Sopot in 2018. This has been achieved with the following aims:

1. Describing the problem of data transformation in Poland when using data from optoelectronic and hydroacoustic devices. The devices and systems used in hydrographic surveys record diverse data with different spatial reference systems. However, the legislation in Poland requires the data transformation to a specific coordinate system.
2. Characterise the systems and devices used during the measurement campaign conducted in Sopot in 2018.
3. Development of the following transformational models and method:
   - Model for the transformation of ellipsoidal coordinates to plane coordinates in the PL–UTM system;
   - Mathematical model of the seven-parameter transformation (Bursa–Wolf transformation) according to the model of P.S. Dąbrowski et al. [26];
   - Mathematical model of seven-parameter transformation (Bursa–Wolf transformation) in the matrix form;
   - Method for determining the depth in relation to a fixed reference level.
4. Model validation on real data coming from the measurement campaign in Sopot.
5. Comparison of two models of the seven-parameter transformation.

This publication presents the practical and theoretical aspects of the data harmonisation from the coastal area, where this problem is particularly frequent. Monitoring of the coastal zone, including bathymetry and coastal topography, is carried out through hydroacoustic and optoelectronic measurements. In the bathymetric and optoelectronic surveys, devices, as well as systems with different reference systems are used. Accordingly, the development of the coordinate transformation models is advisable. In this study, the transformation models were developed and validated using some data derived from measurements of the tombolo oceanographic phenomenon, carried out in Sopot in 2018.

The use of models for the transformation measurement data will enable accurate and quick georeferencing. Hence, the beneficiaries will also be the users whose data need to be georeferenced. Moreover, the developed models can be used in the preparation of maps by the Maritime Office in Poland.

This publication is structured as follows: The first chapter is the Introduction, which provides the motivation for undertaking of the subject. The second chapter presents a model of the transformation ellipsoidal coordinates to the plane coordinates in the PL–UTM (EPSG:32634) system, a mathematical model of the seven-parameter transformation (Bursa–Wolf transformation) according to the model of P.S. Dąbrowski et al. [26] and according to the adjustment calculus, as well as a method for determining the depth in relation to the fixed reference level. The third chapter presents the result of the coordinate transformation, obtained based on real data. The next chapter is the discussion. The paper concludes with final (general) conclusions which summarise the content.

2. Materials and Methods

2.1. GNSS RTK, TLS, UAV and USV Measurement Data

The implementation and validation the mathematical models of the coordinate transformations derived from the GNSS, hydroacoustic, optoelectronic and TLS systems, as well as instruments conducted for the data come from measurements of the tombolo oceanographic phenomenon, carried out in Sopot in 2018 [20–22] (Figure 1).

Figure 1. Map showing the measured waterbodies during the oceanographic phenomenon campaign conducted in Sopot in 2018.

It should be mentioned that the measurements conducted by the USV were burdened with additional errors resulting from the influence of hydrometeorological conditions on the vehicle. To minimise their impact, measurements were taken at sea states 1–2 in the

Douglas scale and at a wind strength of 3 in the Beaufort scale. The meteorological and oceanographic data were provided by the Institute of Metrology and Water Management (IMGW–PIB). The article does not refer to the influence of hydrometeorological conditions, which is the accepted limitation.

The devices and systems used during the measurement campaign are characterised below:

- GNSS Real Time Kinematic (RTK)—a Trimble R10 receiver was used to record the so-called control points. Initially, the control points had plane coordinates in the PL–2000 system and heights in the normal height system. Nevertheless, the plane coordinates were transformed to the PL–UTM system (U34 zone) in the post-processing mode. Furthermore, the GNSS RTK receiver was the positioning system of the USV. The coordinates of the unmanned surface vehicle position and the points measured by the echo sounder were also recorded in the PL–2000 system and the PL–KRON86–NH system. The control points and USV position were determined using the differential GNSS RTK technique. Corrections were obtained from the commercial GNSS geodetic network—VRSNet.pl. The reference station of the VRSNet.pl network located in Gdańsk was used;
- TLS—the TLS point cloud was generated using a Trimble TX–8 laser scanner. The measurement of the TLS included 27 sites separated by a 60 m distance. The registration error of 27-point clouds based on spherical markers was 2.5 mm. The resulting point cloud had an undetermined local coordinate system from the first measurement station. The set of spatial data was subjected to the georeferencing process based on the previously measured, so-called control points;
- USV—the survey of the seabed near the Sopot pier was carried out by an USV with a Trimble R10 receiver and a SonarMite Single Beam Echo Sounder (SBES), which in turn allowed the measured depths to be assigned coordinates from differential GNSS RTK measurements. Therefore, no georeferencing process was necessary for the bathymetric data. However, it was necessary to relate the depth to the chart datum for the selected height system. The target height systems were PL–KRON86–NH and PL–EVRF2007–NH;
- UAV—the measured point cloud by an UAV DJI Mavic 2 Pro, equipped with a photogrammetric camera and a Global Positioning System (GPS) receiver, obtained data in the form of coordinates of the Polish national plane coordinate system (PL–2000) and ellipsoidal heights. The photos were assigned coordinates derived from the navigation sensors of the unmanned aerial vehicle. The UAV mission with the DJI Mavic Pro drone was carried out at an altitude of 60 m. The photogrammetric flight in the 2018 campaign was planned and executed according to the double grid plan. The coverage longitudinal of the photo was 80%, and the same was for the coverage traverse. Georeferencing and processing were conducted in the Pix4D Mapper.

As can be seen, the data derived from the GNSS RTK system and the UAV were originally recorded in the PL–2000 system, which is used for the purposes of compiling maps at scales greater than 1:10,000, in particular the cadastral and master map [24]. Furthermore, the height data from the UAV were recorded in the ellipsoid height system, while the height coordinates from the TLS point cloud were saved in an undetermined local coordination system. Nevertheless, hydrographic survey result compilations should be prepared in the PL–UTM system, as they are used for the purposes of issuing standard cartographic compilations at scales ranging from 1:10,000 to 1:250,000, nautical charts and other maps intended for national security and defense purposes [24]. The PL–UTM projection is characterised by the occurrence of slight distortions in the selected, narrow meridian strip and consists in projecting points (expressed in an angular measure) from the World Geodetic System 1984 (WGS–84) rotational ellipsoid (spheroid) surface onto the plane surface using the Gauss–Krüger transformation that is commonly applied in surveying [27].

Moreover, the height systems valid in Poland are PL–KRON86–NH and PL–EVRF2007–NH [24]. Therefore, it is reasonable to elaborate the data covering the coastal zone in the PL–UTM system, as well as the depth and height in the normal height system. Therefore, the authors of the article transformed the plane coordinates in the primary system (PL–2000) into the PL–UTM system and the height coordinates in the local system into the height system (PL–KRON86–NH). Furthermore, a method was developed for determining the depth in relation to the normal height systems used in Poland.

An important aspect of this harmonisation was carrying out the transformation of the height coordinates. TLS recorded 3D data in an undetermined local coordinate system. Thanks to the GNSS satellite measurement on the control points, it was possible to achieve georeferencing for the generated point cloud, and thus determine the height in the PL–KRON86–NH system. The georeferencing was performed based on two seven-parameter transformation models and the assumption that the marker coordinates were determined in the PL–UTM system.

2.2. Model for the Transformation Ellipsoidal Coordinates to Plane Coordinates in the PL–UTM System

Marine and land navigation are based on the determination of current coordinates in the WGS–84 system [19,27]. However, maps are usually compiled in different coordinate systems. Consequently, there is a problem with the secondary use of data, e.g., compiling nautical charts. According to the Polish National Spatial Reference System, the target system for nautical charts is the UTM [24]. The plane coordinates in the UTM system are created based on the mathematical alignment of points in the reference ellipsoid WGS–84 on the plane and are based on similar mathematical principles as the Gauss–Krüger projection. This means that the coordinates recorded in the geodetic coordinate system WGS–84 can be converted to the PL–UTM system using a modified Gauss–Krüger projection [28]. Figure 2 introduces the model for the transformation of the ellipsoidal coordinates to the plane coordinates in the PL–UTM system flowchart.
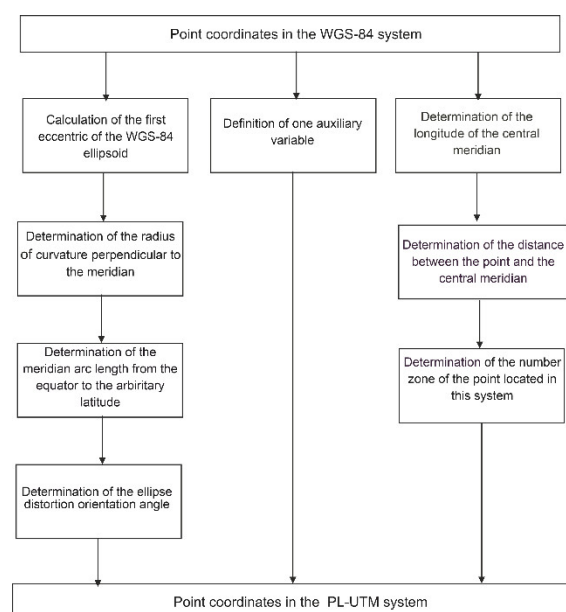
Figure 2. Flowchart showing steps of model for the transformation ellipsoidal coordinates to plane coordinates in the PL–UTM system.

In order to transform the coordinates from the WGS–84 system (B,L) (°) to the PL–UTM system (x_{PL-UTM}, y_{PL-UTM}) (m), it is necessary to start from the calculation of the first eccentric of the WGS–84 ellipsoid (–), which is the reference plane for the PL–UTM system [29,30]:

$$e = \sqrt{\frac{a^2 - b^2}{a^2}} \tag{1}$$

where:

a=6,378,137.000 m—length of the semi-major axis of the WGS–84 ellipsoid,

b=6,356,752.3142452 m—length of the semi-minor axis of the WGS–84 ellipsoid.

In the next computational step, it is necessary to determine the radius of curvature perpendicular to the meridian (N) (m) using the following relationship [29,30]:

$$N = \frac{a}{\sqrt{1 - e^2 \cdot \sin^2(B)}} \tag{2}$$

The meridian arc length from the equator to the arbitrary latitude ($S(B)$) (m) can then be determined using the following formula [29,30]:

$$S(B) = \int_0^B \frac{a \cdot (1 - e^2)}{\sqrt{\left[1 - e^2 \cdot \sin^2(B)\right]^3}} dB \tag{3}$$

The longitude of the central meridian in the PL–UTM system (L_0) (°), in which the point with a length L is located, then needs to be determined [29,30]:

$$L_0 = \begin{cases} 15° & for & L > 12° \wedge L \le 18° \\ 21° & for & L > 18° \wedge L \le 24° \\ 27° & for & L > 24° \wedge L \le 30° \end{cases} \tag{4}$$

The above formula can be used to determine the distance between the point and the central meridian (ΔL) (rad) [29,30]:

$$\Delta L = L - L_0 \tag{5}$$

In order to transform the coordinates to the PL–UTM system, it is necessary to determine the number zone of the point located in this system (*Zone*) (–). To achieve this, the numbering of the zone for the six-degree system PL–1942 needs to be used (6) [29,30]:

$$Zone = \begin{cases} 3 & for & L_0 = 15° \\ 4 & for & L_0 = 21° \\ 5 & for & L_0 = 27° \end{cases} \tag{6}$$

Additionally, it will be necessary to define one auxiliary variable t (–) using the following relationship [29,30]:

$$t = \tan(B) \tag{7}$$

Furthermore, it is necessary to determine the ellipse distortion orientation angle (η) (–) using the formula below [29,30]:

$$\eta = \sqrt{\frac{e^2 \cdot \cos^2(B)}{1 - e^2}} \tag{8}$$

Only then can the $x_{PL–UTM}$, $y_{PL–UTM}$ coordinates be determined. The angular coordinates were converted into the Cartesian coordinates based on the following mathematical relationships [31]:

$$x_{PL-UTM} = m_0 \cdot N \cdot \left[\frac{S(B)}{N} + \frac{(\Delta L)^2}{2} \cdot \sin(B) \cdot \cos(B) + \right.$$

$$+ \frac{(\Delta L)^4}{24} \cdot \sin(B) \cdot \cos^3(B) \cdot (5 - t^2 + 9 \cdot \eta^2 + 4 \cdot \eta^4) +$$

$$\left. + \frac{(\Delta L)^6}{720} \cdot \sin(B) \cdot \cos^5(B) \cdot (61 - 58 \cdot t^2 + t^4) \right] \tag{9}$$

$$y_{PL-UTM} = m_0 \cdot N \cdot \left[\Delta L \cdot \cos(B) + \frac{(\Delta L)^3}{6} \cdot \cos^3(B) \cdot (1 - t^2 + \eta^2) + \right.$$

$$\left. + \frac{(\Delta L)^5}{120} \cdot \cos^5(B) \cdot (5 - 18 \cdot t^2 + t^4 + 14 \cdot \eta^2 - 58 \cdot \eta^2 \cdot t^2) \right] + \tag{10}$$

$$+ 500000 + Zone \cdot 1000000$$

where:

$m_0 = 0.9996$ — scale factor in the PL–UTM system (–).

2.3. Mathematical Model for Seven-parameter Transformation (Bursa–Wolf transformation) According to the P.S. Dąbrowski et al. Model

The Bursa–Wolf transformation, also referred to as the three-dimensional (3D) conformal transformation, is a commonly used coordinate calculation method applied in photogrammetry and surveying [32]. The main advantage of this method is the ability to transform 3D coordinates. It involves the coordinate transformation based on the previously determined parameters, such as rotation matrices, translation vectors and the scale factor. These parameters are calculated through the relationships between the points recorded in two systems, primary and secondary (Figure 3).
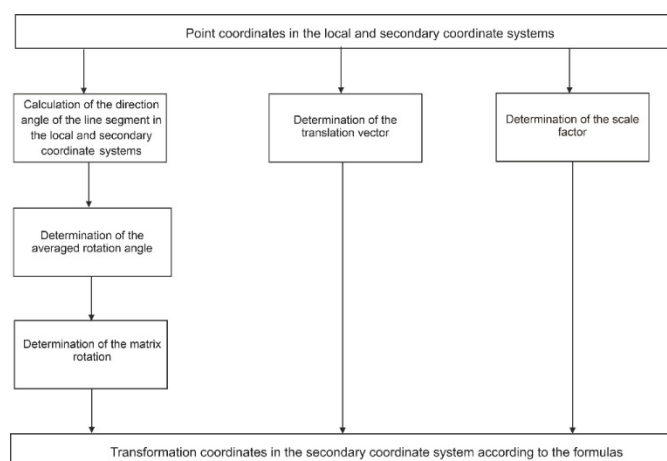
Figure 3. Flowchart showing steps of mathematical model for seven-parameter transformation (Bursa–Wolf transformation) according to the model of P.S. Dąbrowski et al.

In order to achieve high accuracy, the point coordinates are determined by the RTK measurements method [33]. However, it should be noted that the accuracy of data transformation based on fitting depends on the number of determined control points. The reference points must be equally distributed, and their number should be at least 6.

The seven-parameter transformation model is based on the determination of individual parameters: three rotation matrices (R), the scale factor (S) and three translation vectors ($\bar{T}$). Figure 4 shows a diagram that illustrates the seven-parameter transformation parameters; X,Y,Z are the coordinates of a point, and X',Y',Z' are the coordinates after

transformation; R_x,R_y,R_z describe three rotation matrices; $\overline{T}_x$, $\overline{T}_y$, $\overline{T}_z$ are three translation vectors; P is a scale factor.
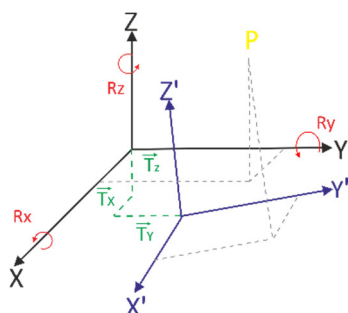
Figure 4. Diagram of the seven-parameter transformation parameters. Own study based on [34].

The first stage of the work on the model development involves the determination of the rotation matrix, i.e., the rotation of the vector in a Euclidean space. The incli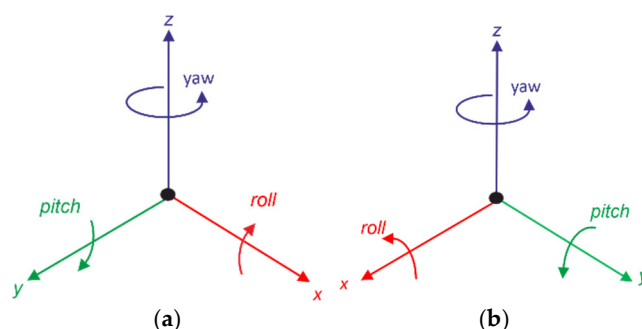nation of coordinate systems is most often determined using the Euler angles. These angles represent the successive rotations that need to be performed in order to make the axis of the local coordinate system cover the axis the of secondary coordinate system. In many cases, the measurement techniques based on aerial drones use Inertial Navigation Systems (INS), which provide information on the angles of the inertial reference system (Figure 5).

Three-dimensional spatial data are characterised by three angles of rotation around the three axes of the local coordinate systems. Figure 5 shows a diagram of the location of the rotation angles around the three Roll Pitch Yaw (RPY) axes.

Figure 5. Diagram the location of three rotation angles around the RPY axes, related to the Inertial Measurement Unit (IMU). Left-handed system (**a**), right-handed system (**b**). Own study based on [35].

Nevertheless, the rotation angle value can be calculated based on the direction angles [36]:

$$\delta_i' = \arctan\left(\frac{y'_{k_i} - y'_{p_i}}{x'_{k_i} - x'_{p_i}}\right) \tag{11}$$

$$\delta_i'' = \arctan\left(\frac{y''_{k_i} - y''_{p_i}}{x''_{k_i} - x''_{p_i}}\right) \tag{12}$$

where:

i—numbering of the line segment (–);

δ_i'—direction angle of the i-th line segment in the local coordinate system (°);

$\delta_i^{''}$ —direction angle of the *i*-th line segment in the secondary coordinate system (°);

$x_{p_i}^{'}, y_{p_i}^{'}$ —coordinates of the starting point of the *i*-th line segment in the local coordinate system (m);

$x_{k_i}^{'}, y_{k_i}^{'}$ —coordinates of the end point of the *i*-th line segment in the secondary coordinate system (m);

$x_{p_i}^{''}, y_{p_i}^{''}$ —coordinates of the starting point of the *i*-th line segment in the local coordinate system (m);

$x_{k_i}^{''}, y_{k_i}^{''}$ —coordinates of the end point of the *i*-th line segment in the secondary coordinate system (m).

The determined direction angles will enable the calculation of the averaged rotation angle (θ) (°):

$$\theta = \frac{\sum_{i=1}^{n}\left(\delta_i^{'} - \delta_i^{''}\right)}{n} \tag{13}$$

where:

n—number of segments (–).

The recorded RPY angles from the IMU are necessary to determine the rotation matrix, which consists of elementary rotation matrices. In the original formulation of the seven-parameter transformation model [37–39], three elementary matrices of the rotation around the axes OX, OY and OZ of the three-dimensional coordinate system are (R_x,R_y,R_z) (–), provided in the following order:

$$R_x(\theta) = \begin{pmatrix} 1 & 0 & 0 \\ 0 & \cos\theta & \sin\theta \\ 0 & -\sin\theta & \cos\theta \end{pmatrix} \tag{14}$$

$$R_y(\theta) = \begin{pmatrix} \cos\theta & 0 & -\sin\theta \\ 0 & 1 & 0 \\ \sin\theta & 0 & \cos\theta \end{pmatrix} \tag{15}$$

$$R_z(\theta) = \begin{pmatrix} \cos\theta & \sin\theta & 0 \\ -\sin\theta & \cos\theta & 0 \\ 0 & 0 & 1 \end{pmatrix} \tag{16}$$

Since the right-handed system is most commonly used to determine the location of objects in the space, the rotation matrices are described using the functions of the rotation angles around the axes in the right-handed system.

The aircraft complete rotation matrix (R) (–) is obtained by multiplying the elementary matrices of the rotation around successive axes [32]:

$$R = R_x(\theta) \cdot R_y(\theta) \cdot R_z(\theta) \tag{17}$$

After performing the dataset rotation, it is necessary to shift the rotated dataset by the translation vector ($\vec{T}$) (m):

$$\vec{T}_x = \frac{\sum_{j=1}^{l}\left(x_j^{'} - x_j^{''}\cos(\theta) + y_j^{''}\sin(\theta)\right)}{l} \tag{18}$$

$$\vec{T}_y = \frac{\sum_{j=1}^{l}\left(y_j' - x_j''\sin(\theta) - y_j''\cos(\theta)\right)}{l} \tag{19}$$

$$\vec{T}_z = \frac{\sum_{j=1}^{l}\left(z_j' - z_j''\right)}{l} \tag{20}$$

where:

j—numbering of measurement (TLS) and reference points (GNSS RTK) (–);

x_j', y_j', z_j' —measurement point coordinates in the local coordinate system (m);

x_j'', y_j'', z_j'' —reference point coordinates in the secondary coordinate system (m);

l—number of measurement and reference points (–).

The final stage in the development of the seven-parameter transformation model involves the determination of the scale factor (S) (–). This factor is the quotient of the distance between two subsequent points expressed in both the local and secondary coordinate system:

$$S = \frac{\sum_{j=1}^{l-1}\left(\dfrac{d_j'}{d_j''}\right)}{l-1} \tag{21}$$

where:

d_j' —distance between two subsequent measurement points expressed in the local coordinate system (m);

d_j'' —distance between two subsequent reference points expressed in the secondary coordinate system (m).

The distance between two subsequent points can be determined using the following relationships:

$$d_j' = \sqrt{\left(x_{j+1}' - x_j'\right)^2 + \left(y_{j+1}' - y_j'\right)^2} \tag{22}$$

$$d_j'' = \sqrt{\left(x_{j+1}'' - x_j''\right)^2 + \left(y_{j+1}'' - y_j''\right)^2} \tag{23}$$

After determining the elementary rotation matrices, translation vectors and the scale factor, the transformation process may begin. Keeping the remaining indications, such as those in the previous formulas, the transformation for a single coordinate is expressed by the following relationship:

$$x_j^d = S \cdot R_x(\theta) \cdot x_j' + \vec{T_x} \tag{24}$$

$$y_j^d = S \cdot R_y(\theta) \cdot y_j' + \vec{T_y} \tag{25}$$

$$z_j^d = S \cdot R_z(\theta) \cdot z_j' + \vec{T_z} \tag{26}$$

where:

x_j^d, y_j^d, z_j^d —coordinates of the j-th point, determined according to the model of P.S. Dąbrowski et al. in the secondary coordinate system (m).

The described transformation Formulas (24)–(26) are used when only the S scale factor is calculated. On the other hand, the entire scale factor (M) (–) can be determined using the following equation:

$$M = 1 + S \qquad (27)$$

In order to determine the rotation matrices, scale factor and three translation vectors, a spatial dataset is required. All of the above-mentioned parameters are determined individually for each coordinate. Then, the arithmetic mean of the above parameters is calculated, which allows to obtain the best approximation of the determined value. The disadvantage of this transformation is its computational complexity.

2.4. Mathematical Model of Seven-parameter Transformation (Bursa–Wolf Transformation) in the Matrix Form

Transformations of the spatial coordinates are carried out by different methods. One of the methods is transformation using a matrix, which enables the solution of an equations system with multiple unknowns. The transformation algorithm in the matrix form was developed based on the parametric method (Figure 6).
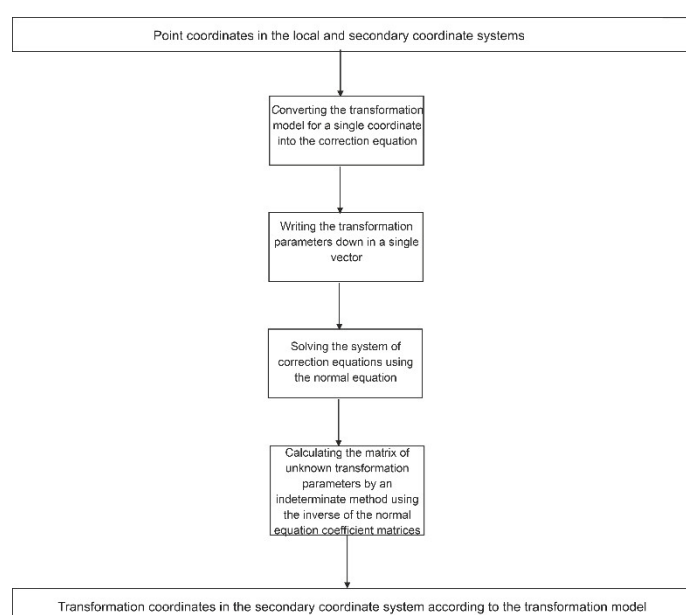
Figure 6. Flowchart showing steps of mathematical model of seven-parameter transformation (Bursa–Wolf transformation) in the matrix form.

In order to understand the nature of the parametric method, it is important to know that the measurements and their results never lead to knowledge of the real values, since each survey is affected by a variety of errors resulting from the adopted method and the used systems and measuring devices [40,41]. Due to this characteristic, the unknown parameters can be determined based on measurement results and the associated errors.

The notation of the measurement error equation (*V*) (–) is calculated using the formula [42]:

$$V = A \cdot X + K \qquad (28)$$

where:

A—matrix of the correction equation coefficients (–);

X—matrix of the unknown transformation parameters (–);

K—matrix of the constant term (–).

On the other hand, the transformation model for a single coordinate can be written as follows [34]:

$$\begin{bmatrix} x_j^r \\ y_j^r \\ z_j^r \end{bmatrix} = \begin{bmatrix} \mu & \gamma & -\beta \\ -\gamma & \mu & \alpha \\ \beta & -\alpha & \mu \end{bmatrix} \cdot \begin{bmatrix} x_j^{'} \\ y_j^{'} \\ z_j^{'} \end{bmatrix} + \begin{bmatrix} x_0 \\ y_0 \\ z_0 \end{bmatrix} \tag{29}$$

where:

x_j^r, y_j^r, z_j^r —coordinates of the *j*-th point, determined according to the seven-parameter transformation model in the secondary coordinate system (m);

$x_j^{'}, y_j^{'}, z_j^{'}$ —coordinates of the *j*-th measurement point in the local coordinate system (m);

α, β, γ —elementary matrices of the rotation around the OX, OY and OZ axes the three-dimensional coordinate system (–);

μ —scale factor (–);

x_0, y_0, z_0 —three components of the translation vector (m).

Converting the transformation model for a single coordinate into the correction equation, another equation was obtained:

$$\begin{bmatrix} v_x \\ v_y \\ v_z \end{bmatrix} = \begin{bmatrix} \mu & \gamma & -\beta \\ -\gamma & \mu & \alpha \\ \beta & -\alpha & \mu \end{bmatrix} \cdot \begin{bmatrix} x_j^{'} \\ y_j^{'} \\ z_j^{'} \end{bmatrix} + \begin{bmatrix} x_0 \\ y_0 \\ z_0 \end{bmatrix} + \begin{bmatrix} x_j^{'} \\ y_j^{'} \\ z_j^{'} \end{bmatrix} - \begin{bmatrix} x_j^r \\ y_j^r \\ z_j^r \end{bmatrix} \tag{30}$$

where:

v_x, v_y, v_z —correction vectors of the *x*, *y* and *z* coordinates (–).

By writing the transformation parameters down in a single vector, the following equation was obtained:

$$\begin{bmatrix} v_x \\ v_y \\ v_z \end{bmatrix} = \begin{bmatrix} x_j^{'} & 0 & -z_j^{'} & y_j^{'} & 1 & 0 & 0 \\ y_j^{'} & z_j^{'} & 0 & -x_j^{'} & 0 & 1 & 0 \\ z_j^{'} & -y_j^{'} & x_j^{'} & 0 & 0 & 0 & 1 \end{bmatrix} \cdot \begin{bmatrix} \mu \\ \alpha \\ \beta \\ \gamma \\ x_0 \\ y_0 \\ z_0 \end{bmatrix} + \begin{bmatrix} x_j^{'} \\ y_j^{'} \\ z_j^{'} \end{bmatrix} - \begin{bmatrix} x_j^r \\ y_j^r \\ z_j^r \end{bmatrix} \tag{31}$$

If the system of correction equations contains more equations than the searched transformation parameters, they can be solved using a normal equation:

$$A^T A \cdot X + A^T K = 0 \tag{32}$$

Using the previous functional relationship (31), the matrix of the unknown transformation parameters can be calculated by an indeterminate method using the inverse of the normal equation coefficient matrices:

$$X = -(A^T A)^{-1} \cdot A^T K \tag{33}$$

2.5. Method for Determining the Depth in Relation to a Fixed Reference Level

Another important method in the integration of data from hydroacoustic and optoelectronic systems is the method for determining the depth in relation to a fixed reference level. It was originally developed for the purposes of the tombolo measurement campaign conducted in 2018. The method presented above considers the differences in water levels during surveys (Figure 7).
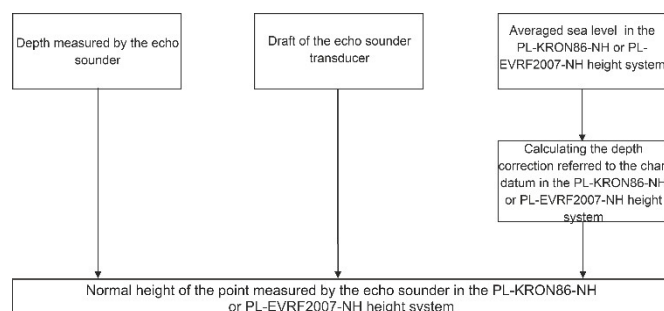
Figure 7. Flowchart showing steps of method for determining the depth in relation to a fixed reference level.

The normal height of the point measured using an echo sounder in the PL–KRON86–NH or PL–EVRF2007–NH system (cm) is calculated using the following formula [43]:

$$H_{PL-KRON86-NH} = -\left(d + \Delta d_E \pm \Delta d_{PL-KRON86-NH}\right) \tag{34}$$

$$H_{PL-EVRF2007-NH} = -\left(d + \Delta d_E \pm \Delta d_{PL-EVRF2007-NH}\right) \tag{35}$$

where:

$H_{PL-KRON86-NH}$—normal height of the point measured by the echo sounder in the PL–KRON86–NH system (cm);

$H_{PL-EVRF2007-NH}$—normal height of the point measured by the echo sounder in the PL–EVRF2007–NH system (cm);

d—depth measured by the echo sounder (cm);

Δd_E—draft of the echo sounder transducer (cm);

$\Delta d_{PL-KRON86-NH}$—depth correction referred to the chart datum in the PL–KRON86–NH system (cm), which needs to be added where the averaged water level ($\bar{d}_{SW}$) does not exceed 508 cm; otherwise, it needs to be subtracted;

$\Delta d_{PL-EVRF2007-NH}$—depth correction referred to the chart datum in the PL–EVRF2007–NH system (cm), which needs to be added where the averaged water level ($\bar{d}_{SW}$) does not exceed 500 cm; otherwise, it needs to be subtracted.

It should be noted, however, that the depth correction Δd is defined as follows [43]:

$$\Delta d_{PL-KRON86-NH} = 508\,cm - \bar{d}_{SW_{PL-KRON86-NH}} \tag{36}$$

$$\Delta d_{PL-EVRF2007-NH} = 500\,cm - \bar{d}_{SW_{PL-EVRF2007-NH}} \tag{37}$$

where:

$\bar{d}_{SW_{PL-KRON86-NH}}$ —averaged sea level observed on a tide gauge between consecutive full hours in the PL–KRON86–NH system (cm);

$\bar{d}_{SW_{PL-EVRF2007-NH}}$ —averaged sea level observed on a tide gauge between consecutive full hours in the PL–EVRF2007–NH system (cm).

The depth correction is determined by the current sea level, which is read in relation to the chart datum. In Poland, most gauging stations have a chart datum for the Kronstad height system amounts to 508 cm and 500 cm for the Amsterdam height system. The sea level observed on the tide gauge between consecutive full hours is usually averaged. More frequent sea level readings can be obtained from limnigraph. When determining the depth correction, an important factor is the choice of the hydrometeorological station, which should be located as close as possible to the bathymetric measurement site. If no hydrometeorological station is located in the vicinity, the water level must be read from the nearest staff gauge, which is shown in Figure 8.
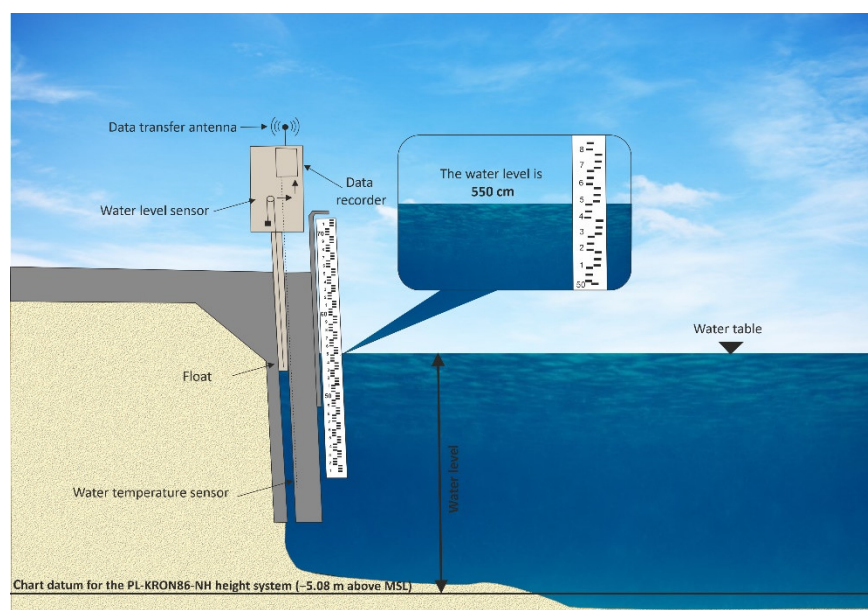
Figure 8. Diagram of water level surveys and temperature measurements carried out by IMGW–PIB.

3. Data Compilation

3.1. Transformation Ellipsoidal Coordinates to Plane Coordinates in the PL–UTM System

The coordinates of the reference points (GNSS RTK) were recorded during the measurement campaign of the oceanographic tombolo phenomenon in Sopot. Initially, they were measured in the PL–2000 plane coordinate system in order to perform georeferencing. Therefore, the coordinates had to be transformed from the PL–2000 plane coordinate system to the WGS–84 coordinate system and then to the PL–UTM plane coordinate system. The control point coordinates in the WGS–84 and PL–UTM systems are listed in Table 1.

Table 1. Coordinates of the reference points in the coordinate system adopted as the primary coordinates (WGS–84) and coordinates of the reference points in the UTM system for the zone 34U.

No.	Primary System (WGS–84)		Secondary System (PL–UTM)	
	B (°)	*L* (°)	Easting (m)	Northing (m)
1	54°26′42.420″	18°34′24.908″	4,342,666.411	6,035,758.415
2	54°26′42.068″	18°34′23.533″	4,342,641.280	6,035,748.376
3	54°26′41.737″	18°35′22.207″	4,342,617.049	6,035,739.002
4	54°26′48.909″	18°34′19.232″	4,342,571.115	6,035,962.427
5	54°26′48.493″	18°34′18.361″	4,342,554.995	6,035,950.142
6	54°26′56.406″	18°34′9.836″	4,342,409.931	6,036,199.924
7	54°26′56.195″	18°34′9.000″	4,342,394.651	6,036,193.918
8	54°26′55.969″	18°34′8.221″	4,342,380.376	6,036,187.421

The computational work started with the determination of the parameter describing the WGS–84 ellipsoid (the first eccentric), which is a reference plane for the PL–UTM system. A value of 0.0818 was obtained. Further on, the radius of curvature perpendicular to the meridian (N) (m), and the meridian arc length from the equator to the arbitrary latitude ($S(B)$) (m) for the reference points, were calculated (Table 2).

Table 2. Values of the radiuses of curvature perpendicular to the meridian (N) and the meridian arc lengths from the equator to the arbitrary latitude ($S(B)$) for the reference points, as well as the difference in longitude between the reference points in the WGS–84 system and the points with a length of L_0 (ΔL).

No.	N (m)	$S(B)$ (m)	ΔL (rad)
1	6,392,314.458	6,035,461.584	−0.042
2	6,392,314.423	6,035,450.684	−0.042
3	6,392,314.391	6,035,440.480	−0.042
4	6,392,315.098	6,035,662.210	−0.042
5	6,392,315.057	6,035,649.376	−0.042
6	6,392,315.837	6,035,894.028	−0.042
7	6,392,315.816	6,035,887.497	−0.042
8	6,392,315.794	6,035,880.511	−0.042

As mentioned in Section 2.2, the UTM projection is based on similar mathematical principles as the Gauss–Krüger projection. One of the differences is that the projection divides the ellipsoid surface into 60 zones of 6° each. This functional relationship enables the determination of both the longitude of the central meridian and the number zone in the PL–UTM system. The reference points measured during the measurement campaign conducted in Sopot are located in zone 4, which corresponds to the central meridian of 21°. Further on, this information was used to determine the distance between the point and the central meridian (ΔL) (rad) (Table 2).

Another parameter needed for the transformation of the ellipsoidal coordinates is the central meridian scale factor. In the Gauss–Krüger projection, the central meridian is faithfully represented, while in the UTM projection, the scale factor for the central meridian of each zone is 0.9996 [29]. The transformation additionally assumes defining a single auxiliary variable t (−) and determining the ellipse distortion orientation angle (η) (−).

After substituting the determined parameters into Formulas (9) and (10), the following coordinates of the reference points in the UTM system for the zone 34U were obtained (Table 1).

3.2. The Method of P.S. Dąbrowski et al.

The method of P.S. Dąbrowski et al. used the data derived from the tombolo measurement campaign conducted in Sopot, particularly the point cloud recorded by terrestrial laser scanning in the local system (TLS) and the reference point coordinates in the secondary system (PL–UTM/PL–KRON86–NH). Table 3 summarises the coordinates of the measurement and reference points.

Table 3. Measurement point coordinates in the local system and reference point coordinates in the secondary system.

No.	Measurement Point Coordinates (TLS)			Reference Point Coordinates (PL–UTM/PL–KRON86–NH)		
	x' (m)	y' (m)	z' (m)	Easting (m)	Northing (m)	$H_{PL-KRON86-NH}$ (m)
1	5.625	−58.129	−1.980	4,342,666.411	6,035,758.415	1.136
2	22.044	−36.590	−2.140	4,342,641.280	6,035,748.376	0.977
3	38.010	−16.104	−1.620	4,342,617.049	6,035,739.002	1.483
4	192.181	−184.240	−1.810	4,342,571.115	6,035,962.427	1.278
5	199.701	−165.421	−1.740	4,342,554.995	6,035,950.142	1.351
6	452.511	−305.242	−1.630	4,342,409.931	6,036,199.924	1.447
7	462.537	−292.243	−1.910	4,342,394.651	6,036,193.918	1.159
8	471.434	−279.343	−1.230	4,342,380.376	6,036,187.421	1.834

The first stage of the coordinate transformation by the method of P.S. Dąbrowski et al. involved the calculation of the averaged rotation angle (θ) (rad). To this end, the direction angles (δ) (°) were determined based on the coordinates in both systems. After determining the two direction angles, it is possible to determine the rotation angle of a single spatial dataset in relation to another one. However, it is recommended to determine the direction angles for a greater number of characteristic lines and to then average the results. The averaged rotation angle for the analysed example was 2.60205 rad (Table 4). Nevertheless, devices equipped with inertial navigation systems (IMU) perform an accelerations measurement and rotation angles in three planes. Hence, direction angles are not always determined [44].

Table 4. Direction and rotation angles of measurement points.

No.	δ' (°)	δ'' (°)	$\delta''-\delta'$ (rad)
1	52°4′6.67″	201°8′59.74″	2.602
2	52°40′55.30″	201°46′28.83″	2.602
3	68°13′6.74″	217°18′37.41″	2.602
4	55°24′22.90″	204°28′17.28″	2.602
5	52°21′26.47″	201°27′32.29″	2.602
		θ	2.602

Further on, the rotation matrix around the OZ axis was calculated (R_z). It is important to note here that the beach surface was scanned using TLS, which was calibrated. Therefore, there was no need to perform additional rotations around the horizontal axes of the coordinate system (R_x, R_y). The matrix of rotation around the OZ axis is provided in Table 5.

Table 5. Rotation matrix around the OZ axis, offset by the averaged rotation angle.

−0.858	0.514	0
−0.514	0.858	0
0	0	1

The next stage involved the calculation of translation vectors, i.e., the difference between the rotated measurement point coordinates in the local system and the reference point coordinates in the secondary system. The arithmetic mean of individual translation vectors was then calculated. Table 6 lists the coordinates of the rotated measurement points selected for georeferencing and their translation vectors.

Table 6. Rotated measurement point coordinates and their translation vectors.

No.	Rotated Measurement Point Coordinates			Coordinates Translation Vector		
	x' (m)	y' (m)	z' (m)	T_x (m)	T_y (m)	T_z (m)
1	25.037	52.761	−1.980	4,342,641.374	6,035,705.653	3.116
2	−0.115	42.717	−2.140	4,342,641.394	6,035,705.659	3.117
3	−24.337	33.344	−1.620	4,342,641.387	6,035,705.658	3.103
4	−70.229	256.799	−1.810	4,342,641.343	6,035,705.628	3.088
5	−86.348	244.517	−1.740	4,342,641.343	6,035,705.625	3.091
6	−231.413	494.355	−1.630	4,342,641.344	6,035,705.569	3.077
7	−246.693	488.353	−1.910	4,342,641.344	6,035,705.564	3.069
8	−260.953	481.857	−1.230	4,342,641.330	6,035,705.564	3.064
				4,342,641.357	6,035,705.615	3.091

The average translation vector of the *x*, *y* and *z* coordinates amounts to 4,342,641.357 m, 6,035,705.615 m and 3.091 m, respectively. This means that the coordinates of the TLS point cloud should be shifted by the values mentioned.

The final stage of calculations consisted of the determination the scale factor, i.e., the calculation the quotient of the line segment length in the local system and the line segment length in the PL–UTM system. Based on the coordinates of the points in both coordinate systems, it was determined that the scale change factor value was 1. After defining all the parameters, the transformation of coordinates to the target system started.

To make sure that the method of P.S. Dąbrowski et al. is suitable for the tested dataset, it was decided to compare the coordinate modelled points with the reference points (Table 7).

Table 7. Measurement point coordinates determined by the method of P.S. Dąbrowski et al., and their differences in relation to the reference point coordinates.

No.	Easting (m)	Northing (m)	$H_{PL-KRON86-NH}$ (m)	dE'[1] (m)	dN'[2] (m)	dHn'[3] (m)
1	4,342,666.395	6,035,758.376	1.111	−0.016	−0.038	−0.025
2	4,342,641.243	6,035,748.332	0.951	−0.037	−0.044	−0.026
3	4,342,617.02	6,035,738.959	1.471	−0.029	−0.043	−0.012
4	4,342,571.129	6,035,962.415	1.281	0.014	−0.012	0.003
5	4,342,555.009	6,035,950.132	1.351	0.014	−0.010	0.000
6	4,342,409.944	6,036,199.970	1.461	0.013	0.046	0.014
7	4,342,394.664	6,036,193.969	1.181	0.013	0.051	0.022
8	4,342,380.404	6,036,187.472	1.861	0.028	0.051	0.027
			RMS	0.022	0.040	0.019

The differences between the eastern [1], northern [2] and height [3] coordinates (PL–UTM) of the measurement points determined by the method of P.S. Dąbrowski et al. and the reference coordinates.

Based on Table 7, it must be concluded that the method of P.S. Dąbrowski et al. showed a high degree of matching for plane coordinates and the height coordinate. The difference between the modelled and reference coordinates did not exceed the following values for the eastern, northern and height coordinates, respectively: 0.037 m, 0.051 m and 0.027 m. However, the standard deviations of the differences between the coordinates modelled by the method of P.S. Dąbrowski et al. and the reference coordinates amounted to the following values for the eastern, northern and height coordinates, respectively: 0.022 m, 0.040 m and 0.019 m.

3.3. Adjustment Calculus Method

The adjustment calculus method used the data from the tombolo measurement campaign conducted in Sopot, in particular the point cloud recorded by terrestrial laser scanning in the local system (TLS) and the reference point coordinates in the secondary system (PL–UTM/PL–KRON86–NH). The parameters were determined based on the measurement and reference point coordinates (Table 3) and the correction equation. These were the correction equation coefficients matrix (*A*) and the constant term matrix (*K*), which are provided in Table 8.

Table 8. Correction equation coefficient matrices and constant term.

Matrix *A*							Matrix *K*
5.625	0	1.980	−58.129	1	0	0	−4,342,660.786
−58.129	−1.980	0	−5.625	0	1	0	−6,035,816.544
−1.980	58.129	5.625	0	0	0	1	−3.116
22.044	0	2.140	−36.59	1	0	0	−4,342,619.236
−36.59	−2.140	0	−22.044	0	1	0	−6,035,784.966
−2.140	36.59	22.044	0	0	0	1	−3.117
38.010	0	1.620	−16.104	1	0	0	−4,342,579.039
−16.104	−1.620	0	−38.010	0	1	0	−6,035,755.106
−1.620	16.104	38.01	0	0	0	1	−3.103
192.181	0	1.810	−184.240	1	0	0	−4,342,378.934

−184.240	−1.810	0	−192.181	0	1	0	−6,036,146.667
−1.810	184.24	192.181	0	0	0	1	−3.088
199.701	0	1.740	−165.421	1	0	0	−4,342,355.294
−165.421	−1.740	0	−199.701	0	1	0	−6,036,115.563
−1.740	165.4210	199.701	0	0	0	1	−3.091
452.511	0	1.630	−305.242	1	0	0	−4,341,957.420
−305.242	−1.630	0	−452.511	0	1	0	−6,036,505.166
−1.630	305.242	452.511	0	0	0	1	−3.077
462.537	0	1.910	−292.243	1	0	0	−4,341,932.114
−292.243	−1.910	0	−462.537	0	1	0	−6,036,486.161
−1.910	292.243	462.537	0	0	0	1	−3.069
471.434	0	1.230	−279.343	1	0	0	−4,341,908.942
−279.343	−1.230	0	−471.434	0	1	0	−6,036,466.764
−1.230	279.343	471.434	0	0	0	1	−3.064

In this case, constant term matrix (K) is the difference between the coordinates recorded in the local coordinate system and the UTM system. Average differences between the eastern, northern and height coordinates of the points registered in the local coordinate system and the coordinates of the measurement points in the UTM system are −4,342,298.971 m, −6,036,134.617 m and −3.091 m.

Further on, the system of correction equations was solved using the normal Equation (32). For this purpose, matrix A was transposed and multiplied the transposed matrix by the previously written matrix A. Additionally, the transposed matrix was multiplied by the matrix K. The matrices transposed in Equation (32) are written down in Table 9.

Table 9. Transposed matrices A^TA and A^TK.

Matrix A^TA							Matrix A^TK
1,042,655.102	0	0	0	1844.043	−1337.312	−14.060	65,541,336.677
0	322,922.040	475,178.200	3016.118	0	−14.060	1337.312	84,863,615.080
0	475,178.200	719,758.309	−2240.114	14.060	0	1844.043	−61,058,755.868
0	3016.118	−2240.114	1,042,629.856	−1337.312	−1844.043	0	16,938,102,653.692
1844.043	0	14.060	−1337.312	8	0	0	−34,738,391.765
−1337.312	−14.060	0	−1844.043	0	8	0	−48,289,076.937
−14.060	1337.312	1844.043	0	0	0	8	−24.725

The final stage of the calculation involved solving the equations system (32) by an indeterminate method using the inverse of the normal equation coefficients. As a result of solving the system of equations, seven parameters of the Bursa–Wolf transformation were obtained (Table 10).

Table 10. Seven-parameter Transformation (Bursa–Wolf Transformation).

Transformation Parameter	Value
μ (−)	1.858
α (rad)	−0.007
β (rad)	0.005
γ (rad)	−0.514
x_0 (m])	4,342,641.377
y_0 (m)	6,035,705.651
z_0 (m)	−0.238

The scale factor is 1.858. This means that data sets have a similar linear scale. However, the value of α, β indicates a small rotation around the OX and OY axes in relation to the two coordinate systems. A high γ value proves that, for the spatial consistency of the data, it is necessary to rotate around the OZ axis.

The obtained parameter values allow for the comparison of the transformation functions. Table 11 summarises the measurement point coordinates determined by the adjustment calculus method and their differences in relation to the reference point coordinates.

Table 11. Measurement point coordinates determined by the adjustment calculus method and their differences in relation to the reference point coordinates.

No.	Easting (m)	Northing (m)	$H_{PL-KRON86-NH}$ (m)	dE'' [1] (m)	dN'' [2] (m)	dHn'' [3] (m)
1	4,342,666.413	6,035,758.424	1.105	0.002	0.009	−0.031
2	4,342,641.267	6,035,748.378	1.468	−0.013	0.002	0.491
3	4,342,617.046	6,035,738.998	1.238	−0.003	−0.004	−0.245
4	4,342,571.125	6,035,962.422	1.071	0.010	−0.005	−0.207
5	4,342,555.009	6,035,950.138	1.174	0.014	−0.004	−0.177
6	4,342,409.92	6,036,199.924	1.436	−0.011	0.000	−0.011
7	4,342,394.645	6,036,193.922	1.813	−0.006	0.004	0.654
8	4,342,380.384	6,036,187.419	1.360	0.008	−0.002	−0.474
			RMS	0.009	0.005	0.359

The differences between the eastern [1], northern [2] and height [3] coordinates (PL–UTM) of the measurement points determined by the adjustment calculus method and the reference coordinates.

Table 11 shows that the adjustment calculus method showed a high degree of matching for the plane coordinates. The difference between the modelled and reference coordinates did not exceed the following values for the eastern, northern and height coordinates (0.013 m, 0.009 m and 0.654 m, respectively). However, the standard deviations of the differences between the coordinates modelled by the adjustment calculus method and the reference coordinates amounted to the following values for the eastern, northern and height coordinates (0.009 m, 0.005 m and 0.359 m, respectively).

4. Discussion

In geodesy and photogrammetry, the most common problem procedure is to move from one coordinate system to the other. The analysed examples of the methods for integrating hydroacoustic and optoelectronic data in [19] indicate the lack of a single data fusion scheme. In all of the schemes, the data fusion was multistage and required the use of commercial software, e.g., ArcGIS, CloudCompare, Eye4Software Coordinate Calculator and VDatum. However, one of the methods [26] contained a transformational model. Therefore, it was implemented and validated. Therefore, this article presents a mathematical description of the procedures used in the data harmonisation process. One of them is the method of P.S. Dąbrowski et al.

The method of P.S. Dąbrowski et al. was applied on a point cloud derived from TLS and on the reference points determined using the GNSS RTK receiver. The point cloud had no georeferencing, while the reference points had georeferencing. The method of P.S. Dąbrowski et al. was originally implemented on the data recorded in the PL–2000 system. In this publication, the method was used on data in the PL–UTM system. Table 12 summarises the absolute error values of the measurement point coordinates in the PL–UTM and PL–2000 systems determined by the method of P.S. Dąbrowski et al.

Table 12. Absolute error values of the measurement point coordinates in the PL–UTM and PL–2000 systems determined by the method of P.S. Dąbrowski et al.

No.	Method of P.S. Dąbrowski et al. (PL–UTM)		Method of P.S. Dąbrowski et al. (PL–2000)	
	dE' (m)	dN' (m)	dE''' [1] (m)	dN''' [2] (m)
1	−0.016	−0.038	0.009	−0.010
2	−0.037	−0.044	−0.009	−0.020
3	−0.029	−0.043	0.002	−0.022
4	0.014	−0.012	0.013	−0.006

5	0.014	−0.010	0.016	−0.005
6	0.013	0.046	−0.016	0.020
7	0.013	0.051	−0.016	0.023
8	0.028	0.051	0.000	0.022
RMS	0.022	0.040	0.012	0.018

The differences between the eastern [1] and northern [2] coordinates (PL–2000) of the measurement points determined by the method of P.S. Dąbrowski et al. and the reference coordinates.

The accuracy analysis showed that the best results for the eastern and northern coordinates were obtained for the coordinates recorded by the PL–2000 system. This may be due to the fact that the PL–2000 system is a local system that occurs only in Poland, whereas the PL–UTM system is an international, military navigational plane coordinate system.

The article presents two methods of seven-parameter transformation. It should be noted that the method of P.S. Dąbrowski et al. requires that the user determine the parameters in several stages, although the adjustment calculus method is based on the correction equation. Additionally, the method of P.S. Dąbrowski et al. and the adjustment calculus method involves small number of parameters that are programmable and simple. Moreover, the advantage of the methods is the possibility of using them in order to conduct georeferencing to local systems. However, they are designed to perform coordinate transformation between two geodetic datums without eliminating known distortion, especially in the long-used local geodetic datums.

5. Conclusions

The accuracy analysis showed that the standard deviations of the differences between the coordinates modelled by the method of P.S. Dąbrowski et al. and the reference coordinates amounted to the following values for the eastern, northern and height coordinates: 0.022 m, 0.040 m and 0.019 m, respectively. On the other hand, the standard deviations of the differences between the coordinates modelled by the adjustment calculus method and the reference coordinates amounted to the following values for the eastern, northern and height coordinates: 0.009 m, 0.005 m and 0.359 m, respectively (Table 13).

Table 13. Absolute error values of the measurement point coordinates determined by the method of P.S. Dąbrowski et al. and the adjustment calculus method.

No.	Method of P.S. Dąbrowski et al.			Adjustment Calculus Method		
	dE' (m)	dN' (m)	dH_n''(m)	dE'' (m)	dN'' (m)	dH_n'' (m)
1	−0.016	−0.038	−0.025	0.002	0.009	−0.031
2	−0.037	−0.044	−0.026	−0.013	0.002	0.491
3	−0.029	−0.043	−0.012	−0.003	−0.004	−0.245
4	0.014	−0.012	0.003	0.010	−0.005	−0.207
5	0.014	−0.010	0.000	0.014	−0.004	−0.177
6	0.013	0.046	0.014	−0.011	0.000	−0.011
7	0.013	0.051	0.022	−0.006	0.004	0.654
8	0.028	0.051	0.027	0.008	−0.002	−0.474
RMS	0.022	0.040	0.019	0.009	0.005	0.359

It should be noted that the reference point coordinates were initially recorded in the PL–2000 and PL–KRON86–NH systems. Therefore, for the purposes of this study, the plane coordinates of the reference points were transformed from the PL–2000 system to the PL–UTM system. It is necessary to conduct a measurement campaign in the future in which the point coordinates are determined in the PL–UTM system.

This study has potential limitations. The first limitation of the study is the sample size. The sample size is too small, and so statistical tests are not able to identify significant

relationships within the data set. However, for the purposes of georeferencing, the sample size is appropriate. The second limitation is applying the method. The presented methods will work best on data where the secondary system will be the selected local system. This is due to the accuracy of the coordinate systems. The third limitation concerns the method of P.S. Dąbrowski et al. Depending on the type of data, appropriate rotation matrices must be selected. In the analysed example, the Trimble TX–8 laser scanner on each measurement station was leveled, so the only considered elementary rotation of the TLS point cloud was the rotation around the OZ axis.

On the basis of the collected data, it can be concluded that the most accurate plane coordinates were obtained by the adjustment calculus method. Nevertheless, it was the method of P.S. Dąbrowski et al. that obtained the best results for the height coordinate. It can be assumed that a combination of these two seven-parameter transformation methods would provide the best results. The authors of the current publication are planning to conduct a new measurement campaign using hydroacoustic and optoelectronic devices in the future. Additionally, they are considering the development of a new seven-parameter transformation method based on the synthesis of the two existing methods.

Author Contributions: Conceptualization, O.L., M.S. (Mariusz Specht) and A.S.; Formal analysis, B.S. and A.H.; Investigation, B.S., M.S. (Marcin Stateczny) and S.W.; Methodology, O.L. and M.S. (Mariusz Specht); Supervision, C.S., C.D. and P.D.; Visualization, A.H., M.S. (Marcin Stateczny) and S.W.; Writing—original draft, O.L., M.S. (Mariusz Specht) and A.S.; Writing—review and editing, C.S., C.D. and P.D. All authors have read and agreed to the published version of the manuscript.

Data Availability Statement: Not applicable.

Conflicts of Interest: The authors declare no conflict of interest.

References

1. Stateczny, A.; Włodarczyk-Sielicka, M.; Grońska, D.; Motyl, W. Multibeam Echosounder and LiDAR in Process of 360-degree Numerical Map Production for Restricted Waters with HydroDron. In Proceedings of the Baltic Geodetic Congress 2018 (BGC 2018), Gdańsk, Poland, 21–23 June 2018.
2. Kopacz, Z.; Morgas, W.; Urbanski, J. Hydrography: Its Present State and Future Development. *Int. Hydrogr. Rev.* **2003**, *6*, 69–76.
3. Giordano, F.; Mattei, G.; Parente, C.; Peluso, F.; Santamaria, R. Integrating Sensors into a Marine Drone for Bathymetric 3D Surveys in Shallow Waters. *Sensors* **2016**, *16*, 41.
4. Zwolak, K.; Wigley, R.; Bohan, A.; Zarayskaya, Y.; Bazhenova, E.; Dorshow, W.; Sumiyoshi, M.; Sattiabaruth, S.; Roperez, J.; Proctor, A.; et al. The Autonomous Underwater Vehicle Integrated with the Unmanned Surface Vessel Mapping the Southern Ionian Sea. The Winning Technology Solution of the Shell Ocean Discovery XPRIZE. *Remote Sens.* **2020**, *12*, 1344.
5. Kang, M. Overview of the Applications of Hydroacoustic Methods in South Korea and Fish Abundance Estimation Methods. *Fish. Aquat. Sci.* **2014**, *17*, 369–376.
6. Prošek, J.; Gdulová, K.; Barták, V.; Vojar, J.; Solský, M.; Rocchini, D.; Moudrý, V. Integration of Hyperspectral and LiDAR Data for Mapping Small Water Bodies. *Int. J. Appl. Earth Obs. Geoinf.* **2020**, *92*, 102181.
7. Eren, F.; Pe'eri, S.; Rzhanov, Y.; Ward, L. Bottom Characterization by Using Airborne Lidar Bathymetry (ALB) Waveform Features Obtained from Bottom Return Residual Analysis. *Remote Sens. Environ.* **2018**, *206*, 260–274.
8. Niemeyer, J.; Soergel, U. Opportunities of Airborne Laser Bathymetry for the Monitoring of the Sea Bed on the Baltic Sea Coast. *Int. Arch. Photogramm. Remote Sens. Spat. Inf. Sci.* **2013**, *40*, 179–184.
9. Specht, M.; Wiśniewska, M.; Stateczny, A.; Specht, C.; Szostak, B.; Lewicka, O.; Stateczny, M.; Widźgowski, S.; Halicki, A. Analysis of Methods for Determining Shallow Waterbody Depths Based on Images Taken by Unmanned Aerial Vehicles. *Sensors* **2022**, *22*, 1844.
10. Kasvi, E.; Salmela, J.; Lotsari, E.; Kumpula, T.; Lane, S.N. Comparison of Remote Sensing Based Approaches for Mapping Bathymetry of Shallow, Clear Water Rivers. *Geomorphology* **2019**, *333*, 180–197.
11. Dietrich, J.T. Bathymetric Structure-from-Motion: Extracting Shallow Stream Bathymetry from Multi-View Stereo Photogrammetry. *Earth Surf. Process. Landf.* **2017**, *42*, 355–364.
12. Lubczonek, J.; Kazimierski, W.; Zaniewicz, G.; Lacka, M. Methodology for Combining Data Acquired by Unmanned Surface and Aerial Vehicles to Create Digital Bathymetric Models in Shallow and Ultra-shallow Waters. *Remote Sens.* **2022**, *14*, 105.

13. Karaki, A.A.; Bibuli, M.; Caccia, M.; Ferrando, I.; Gagliolo, S.; Odetti, A.; Sguerso, D. Multi-platforms and Multi-sensors Integrated Survey for the Submerged and Emerged Areas. *J. Mar. Sci. Eng.* **2022**, *10*, 753.

14. Esri. Esri. Available online: https://www.esri.com (accessed on 21 July 2022).

15. Agisoft Metashape. Agisoft. Available online: https://www.agisoft.com (accessed on 21 July 2022).

16. Genchi, S.A.; Vitale, A.J.; Perillo, G.M.E.; Seitz, C.; Delrieux, C.A. Mapping Topobathymetry in a Shallow Tidal Environment Using Low-cost Technology. *Remote Sens.* **2020**, *12*, 1394.

17. Mancini, F.; Dubbini, M.; Gattelli, M.; Stecchi, F.; Fabbri, S.; Gabbianelli, G. Using Unmanned Aerial Vehicles (UAV) for High-resolution Reconstruction of Topography: The Structure from Motion Approach on Coastal Environments. *Remote Sens.* **2013**, *5*, 6880–6898.

18. Cheng, L.; Ma, L.; Cai, W.; Tong, L.; Li, M.; Du, P. Integration of Hyperspectral Imagery and Sparse Sonar Data for Shallow Water Bathymetry Mapping. *IEEE Trans. Geosci. Remote Sens.* **2015**, *53*, 3235–3249.

19. Lewicka, O.; Specht, M.; Stateczny, A.; Specht, C.; Brčić, D.; Jugović, A.; Widźgowski, S.; Wiśniewska, M. Analysis of GNSS, Hydroacoustic and Optoelectronic Data Integration Methods Used in Hydrography. *Sensors* **2021**, *21*, 7831.

20. Masnicki, R.; Specht, C.; Mindykowski, J.; Dąbrowski, P.; Specht, M. Accuracy Analysis of Measuring X-Y-Z Coordinates with Regard to the Investigation of the Tombolo Effect. *Sensors* **2020**, *20*, 1167.

21. Specht, M.; Specht, C.; Lasota, H.; Cywiński, P. Assessment of the Steering Precision of a Hydrographic Unmanned Surface Vessel (USV) along Sounding Profiles Using a Low-cost Multi-Global Navigation Satellite System (GNSS) Receiver Supported Autopilot. *Sensors* **2019**, *19*, 3939.

22. Specht, M.; Specht, C.; Mindykowski, J.; Dąbrowski, P.; Maśnicki, R.; Makar, A. Geospatial Modeling of the Tombolo Phenomenon in Sopot Using Integrated Geodetic and Hydrographic Measurement Methods. *Remote Sens.* **2020**, *12*, 737.

23. Council of Ministers of the Republic of Poland. *Ordinance of the Council of Ministers of 19 December 2019 Amending the Regulation on the National Spatial Reference System*; Council of Ministers of the Republic of Poland: Warsaw, Poland, 2019. (In Polish).

24. Council of Ministers of the Republic of Poland. *Ordinance of the Council of Ministers of 15 October 2012 on the National Spatial Reference System*; Council of Ministers of the Republic of Poland: Warsaw, Poland, 2012. (In Polish).

25. European Parliament, European Council. *Directive 2007/2/EC of the European Parliament and of the Council of 14 March 2007 Establishing an Infrastructure for Spatial Information in the European Community (INSPIRE)*; European Parliament, European Council: Brussels, Belgium, 2007.

26. Dąbrowski, P.S.; Specht, C.; Specht, M.; Burdziakowski, P.; Makar, A.; Lewicka, O. Integration of Multi-source Geospatial Data from GNSS Receivers, Terrestrial Laser Scanners, and Unmanned Aerial Vehicles. *Can. J. Remote. Sens.* **2021**, *47*, 621–634.

27. Grafarend, E. The Optimal Universal Transverse Mercator Projection. In *Geodetic Theory Today*; Sansò, F., Ed.; International Association of Geodesy Symposia; Springer: Berlin/Heidelberg, Germany, 1995; Volume 114, pp. 51–51.

28. Gajderowicz, I. *Mathematical Cartography for Surveyors*; Publishing House of the Academy of Agriculture and Technology in Olsztyn: Olsztyn, Poland, 1991. (In Polish).

29. Gajderowicz, I. *Cartographic Projections: The Basics*; Publishing House of the University of Warmia and Mazury: Olsztyn, Poland, 2009. (In Polish).

30. Kadaj, R.J. Polish Coordinate Systems. Transformation Formulas, Algorithms and Softwares. Available online: http://www.geonet.net.pl/images/2002_12_uklady_wspolrz.pdf (accessed on 21 July 2022).

31. Hofmann-Wellenhof, B.; Lichtenegger, H.; Collins, J. *Global Positioning System: Theory and Practice*; Springer: New York, NY, USA, 1994.

32. Deakin, R.E. A Note on the Bursa-Wolf and Molodensky-Badekas Transformations. *Sch. Math. Geospat. Sci. RMIT Univ.* **2006**, 1–21.

33. Torge, W.; Müller, J. *Geodesy*, 4th ed.; Walter de Gruyter GmbH: Berlin, Germany, 2012.

34. González-Matesanz, J.; Dalda, A.; Malpica, J.A. A Range of ED50-ETRS89 Datum Transformation Models Tested on the Spanish Geodetic Network. *Surv. Rev.* **2006**, *38*, 654–667.

35. Elmquist, A.; Negrut, D. TR-2016-13 Virtual Sensing for Autonomous Vehicle Simulation in Chrono. Available online: https://sbel.wisc.edu/wp-content/uploads/sites/569/2018/05/TR-2016-13.pdf (accessed on 21 July 2022).

36. Feltens, J. Vector Methods to Compute Azimuth, Elevation, Ellipsoidal Normal, and the Cartesian (X, Y, Z) to Geodetic (φ, λ, h) Transformation. *J. Geod.* **2008**, *82*, 493–504.

37. Burša, M. *Základy Kosmické Geodézie. Díl I, Kosmická Geodézie Geometrická*; MNO: Prague, Czechoslovakia, 1967. (In Czechoslovak).

38. Wolf, H. Geometric Connection and Re-orientation of Three-dimensional Triangulation Nets. *Bull. Geod.* **1963**, *37*, 165–169.

39. Wolf, H. Possibilities for the Joint Adjustment of Satellite and Terrestrial Triangulation and Trilateration Network. *DGK*, **1967**, *153*, 93–99.

40. Alcaras, E.; Parente, C.; Vallario, A. The Importance of the Coordinate Transformation Process in Using Heterogeneous Data in Coastal and Marine Geographic Information System. *J. Mar. Sci. Eng.* **2020**, *8*, 708.

41. Huynh, N.D.Q.; Dang, X.T.; Tran, T.B.T. Introduction of EIO Model in TLS Method to Calculate the Coordinates Transformation by Helmert's Formula. *InterConf* **2021**, *87*, 256–266.

42. Szubrycht, T.; Wiśniewski, Z. Identification and Correction Coordinates Beacons Burdened by Thick Error Issue. *Sci. J. Pol. Nav. Acad.* **2004**, *156*, 49–70. (In Polish).

43. Specht, C.; Lewicka, O.; Specht, M.; Dąbrowski, P.; Burdziakowski, P. Methodology for Carrying out Measurements of the Tombolo Geomorphic Landform Using Unmanned Aerial and Surface Vehicles near Sopot Pier, Poland. *J. Mar. Sci. Eng.* **2020**, *8*, 384.

44. Oh, J.; Kim, M. Method to Determine Initial Aiming Azimuth Accuracy Using Acceleration, Gyroscope, and Geomagnetic Sensors. *ICT Express* **2020**, *6*, 117–120.